

# Total cross section of $pp \rightarrow K^+ \Lambda p$ reaction near threshold

O.Grebenyuk\*

Petersburg Nuclear Physics Institute

## Abstract

The total cross sections of the  $pp \rightarrow K^+ \Lambda p$  reaction near threshold measured at the COSY(Juelich) synchrotron using the internal target facility COSY-11 are described in the frame of the model taking into account the one pion and one kaon exchange as well as the final state interaction mechanisms. It is shown that near the threshold all these mechanisms give the compatible contributions, but with the increasing energy the one kaon exchange mechanism becomes the dominating one.

## Introduction

The total cross sections of the  $pp \rightarrow K^+ \Lambda p$  reaction near threshold measured at the COSY(Juelich) synchrotron using the internal target facility COSY-11 [1, 2, 3] present good test for the various models of the associated strangeness production. In Tab. 1 the 13 values of  $\sigma_{tot}(pp \rightarrow K \Lambda p)$  measured at different periods [1, 3] are presented. Let us dwell on some theoretical models of the  $pp \rightarrow K^+ \Lambda p$  reaction. In the paper [4] the parameters of the model presenting the amplitude as a coherent sum

$$M = M_{OPE} + M_{OKE} + M_{FSI(\pi)} + M_{FSI(K)} , \quad (1)$$

---

\*e-mail: oleg@mail.cern.ch

$Q_{pp}$ , GeV	$T_p$ , GeV	$\sigma_{tot}(pp \rightarrow K\Lambda p)$ nb	Reference
0.00068	1.58377	$2.1 \pm 0.2$	[1]
0.00168	1.58648	$13.4 \pm 0.7$	[1]
0.00268	1.58920	$36.6 \pm 2.6$	[1]
0.00368	1.59192	$63.0 \pm 3.1$	[1]
0.00468	1.59464	$92.2 \pm 6.5$	[1]
0.00568	1.59736	$135 \pm 11$	[1]
0.00668	1.60008	$164 \pm 10$	[1]
0.0139	1.62000	$630 \pm 79$	[3]
0.0159	1.62546	$727 \pm 57$	[3]
0.0202	1.63722	$1011 \pm 99$	[3]
0.0301	1.66436	$1366 \pm 247$	[3]
0.0397	1.69079	$2118 \pm 266$	[3]
0.0593	1.74504	$3838 \pm 624$	[3]

Table 1: Total cross sections  $\sigma_{tot}(pp \rightarrow pK\Lambda)$  from [1] and [3].  $Q = W - m_p - m_\Lambda - m_K$  is the excess energy.

had been chosen in order to match the existing total cross sections in the energy interval  $2 < T_p < 6$  GeV [6]<sup>1</sup>. It had been shown, that the main contribution to the total cross sections in this energy interval provides the one kaon exchange mechanism (OKE). Final state interaction (FSI) contribute very little except the region close to the kaon production threshold. The Juelich group [7] also has stated that, in principle,  $K$  exchange alone could explain the total cross section especially after inclusion of FSI effects. However the  $\pi^0$  exchange cannot be neglected near the threshold. It was argued that the experimental data require a destructive interference between  $\pi^0$  and  $K$  exchange contributions. In the paper [8] the detailed study of the chances for identifying the reaction mechanism of strangeness production are performed by considering the  $\pi^0$  and  $K$  exchange diagrams.

The aim of present work is to perform the calculations as accurate as possible using as the amplitude a coherent sum (1), thus following the papers of J.M.Laget [4, 5]. The model, which describes fairly well the total cross section in the wide interval of the excess energy  $Q = W - m_p - m_\Lambda - m_K$  from 0.7 to 500 MeV, is planned to use for the analysis of the proton and

---

<sup>1</sup>In the next Laget's paper [5] the data close to threshold, ( $0.68 \leq Q \leq 6.68$  MeV [1]) are already taken into account.

kaon spectra in  $pp \rightarrow p\Lambda K$  reaction at COSY energies [9].

Although near the threshold the spin flip effects are negligible, the special attention is paid to the complete taking into account of the spin dependence of the considered amplitudes. It allows to make realistic predictions of the polarization observables for intermediate energies, which will be published elsewhere. The Stapp formalism of the  $M$ -functions is the most proper formalism in this case and it is shortly described in the Appendix A.

## 1 The total cross section

The five-fold cross section is equal to

$$\frac{d^5\sigma}{dp_p d\Omega_p d\Omega_K} = \frac{p_p^2 p_K^2}{(2\pi)^5 8E_p} \frac{1}{4p_b m} \frac{1}{|p_K E_\Lambda - p_\Lambda E_K z_{\Lambda K}|} |M|^2, \quad (2)$$

where  $z_{\Lambda K} \equiv \mathbf{p}_K \cdot \mathbf{p}_\Lambda / p_K p_\Lambda$ . The amplitude  $M$  has been also calculated as a coherent sum (1) where the separate contributions in this sum are considered in details in the next sections

From eq.(2) the total cross section reads as

$$\sigma_{tot} = \frac{1}{(2\pi)^5} \frac{1}{32mp_b} \int d^3p_p \int d\Omega_K \frac{p_K^2}{E_p} \frac{1}{|p_K E_\Lambda - p_\Lambda E_K z_{\Lambda K}|} |M|^2. \quad (3)$$

Let  $\mathbf{p}_b$  be the momentum of the beam proton,  $\mathbf{p}_b$  being directed along the z-axis. The total 4-momentum and the squared invariant mass of the system are equal

$$p_{tot} = (E, \mathbf{p}_b) = (m_p + \sqrt{m_p^2 + p_b^2}, \mathbf{p}_b), \quad s = W^2 = p_{tot}^2.$$

The proton momenta are placed then inside the ellipsoid

$$\frac{p_{px}^2 + p_{py}^2}{q_{cm}^2} + \frac{(p_{pz} - p_0)^2}{\left(\frac{E}{W} q_{cm}\right)^2} = 1, \quad (4)$$

where

$$q_{cm}^2 = \frac{(s - (m_p + m_\Lambda + m_K)^2)(s - (m_p - m_\Lambda - m_K)^2)}{4s} \quad (5)$$

is squared c.m. momentum of proton in the case of minimal mass of  $K\Lambda$  sub-system equal to  $m_\Lambda + m_K$  and

$$p_0 \equiv p_b \frac{s + m_p^2 - (m_\Lambda + m_K)^2}{2s}. \quad (6)$$

It is natural to prepare the integral (3) for numerical integration over  $d^3p_p$  by choosing the elliptical coordinates

$$\begin{aligned} p_{px} &= a \sinh u \sin \theta' \cos \phi \\ p_{py} &= a \sinh u \sin \theta' \sin \phi \\ p_{pz} &= p_0 + a \cosh u \cos \theta' , \end{aligned} \tag{7}$$

where

$$a \equiv q_{cm} \frac{p_{tot}}{W} ,$$

and

$$0 \leq u \leq u_{max}$$

with

$$\sinh u_{max} = \frac{W}{p_{tot}} , \quad \cosh u_{max} = \frac{E}{p_{tot}} .$$

The Jacobian of transition from Cartesian to elliptical coordinates is equal to

$$d^3p_p = a^3 (\sinh^2 u + \sin^2 \theta') \sinh u \sin \theta' \, du d\theta' d\phi$$

or

$$d^3p_p = a^3 (\cosh^2 u - x'^2) d \cosh u dx' d\phi . \tag{8}$$

Note that the volume of this ellipsoid is equal to

$$V = \frac{4\pi}{3} q_{cm}^3 \frac{E}{W} .$$

Indeed it is calculated with the Jacobian (8):

$$\begin{aligned} V &= \int d^3p = a^3 \int_1^{\frac{E}{p_{tot}}} d \cosh u \int_{-1}^1 dx \int_0^{2\pi} d\phi (\cosh^2 u - x^2) = \\ &= 2\pi a^3 \int_1^{\frac{E}{p_{tot}}} d \cosh u \left( 2 \cosh^2 u - \frac{2}{3} \right) = \frac{4\pi}{3} q_{cm}^3 \frac{E}{W} \end{aligned}$$

We replace the measure  $d\Omega_K$ , where the angles  $\Omega = (\theta_K, \phi_K)$  of kaon are defined with respect to fixed frame, by  $d\Omega_{K(K\Lambda)}$  with the kaon polar angles defined with respect to momentum of  $K\Lambda$  sub-system. In this case we can

make the trivial integration over azimuthal angle of proton and obtain from eq.(3)

$$\sigma_{tot} = \frac{1}{(2\pi)^4} \frac{1}{32mp_b} a^3 \int_1^{E/p_{tot}} d \cosh u \int_{-1}^1 dx' \int d\Omega_{K(K\Lambda)} (\cosh^2 u - x'^2) \frac{p_K^2}{E_p} \frac{|M|^2}{|p_K E_\Lambda - p_\Lambda E_K z_{\Lambda K}|} . \quad (9)$$

Let the variables of integration in eq.(9) be replaced by variables  $q_i$ ,  $i = 1, 2, 3, 4$  such that  $0 \leq q_i \leq 1$ . Then

$$\begin{aligned} \cosh u &= 1 + \left(\frac{E}{p_b} - 1\right)q_1, & d \cosh u &= \left(\frac{E}{p_b} - 1\right)dq_1, \\ x' &= 1 + 2q_2, & dx' &= 2dq_2, \\ x_K &= 1 + 2q_3, & dx_K &= 2dq_3, \\ \phi_K &= 2\pi q_4, & d\phi_K &= 2\pi dq_4. \end{aligned}$$

Then we can rewrite the eq.(9) as

$$\sigma_{tot} = \frac{1}{(2\pi)^3} \frac{a^3}{8mp_b} \left(\frac{E}{p_b} - 1\right) \int_0^1 dq_1 \int_0^1 dq_2 \int_0^1 dq_3 \int_0^1 dq_4 (\cosh^2 u - x'^2) \frac{p_K^2}{E_p} \frac{|M|^2}{|p_K E_\Lambda - p_\Lambda E_K z_{\Lambda K}|} . \quad (10)$$

With the eq.(10) we have tested the model considered in next sections by using the CERN program RIWIAD, an adaptive multidimensional integration subroutine which permits numerical integration of a large class of functions, in particular those that are irregular at the border of the integration region.

## 2 Pion exchange mechanisms

In what follows the tensor-like notation for the amplitudes with the indices characterizing spin projections is used. The upper and lower indices relate to the final and initial channels, respectively. The same index at the up and down positions stands for a summation over this index. So, the  $pp \rightarrow p\Lambda K^+$  amplitude looks like

$$M_{\sigma_t \sigma_b}^{\sigma_p \sigma_\Lambda}(p_K, p_\Lambda, p_p; p_t, p_b) ,$$

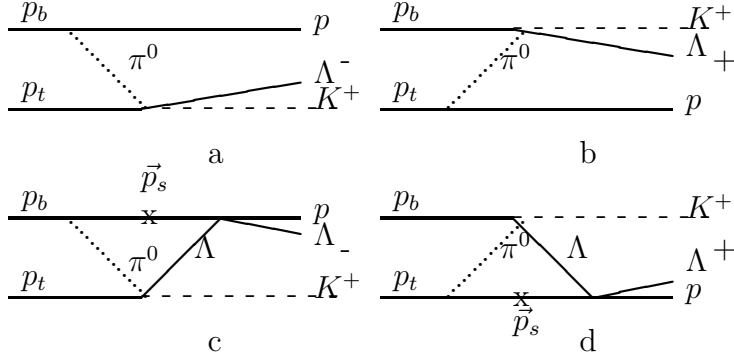


Figure 1: OPE (a,b) and FSI diagrams (c,d)

where  $\sigma_t, \sigma_b, \sigma_p$  and  $\sigma_\Lambda$  are the spin projections of the target, beam, final proton and  $\Lambda$  respectively.  $p_K, p_\Lambda, p_p, p_t, p_b$  are the corresponding momenta.

## 2.1 One Pion Exchange amplitude

The one pion exchange(OPE) graphs are shown in Figs. 1 (a,b). Let us start with the contribution of the graph *a*:

$$i \frac{M_{(\pi^0 p \rightarrow K^+ \Lambda)} \sigma_t^\Lambda(p_\Lambda, p_K; p_t, p_b - p_p) G_{(\pi^0 pp)} \sigma_b^p(p_p, p_b - p_p; p_b)}{t - m_\pi^2}, \quad (11)$$

where  $t = (p_b - p_p)^2 < 0$  is the squared mass of the virtual  $\pi^0$ ,  $M_{(\pi^0 p \rightarrow K^+ \Lambda)}$  is the half-off-shell  $\pi^0 p \rightarrow K^+ \Lambda$  amplitude and  $G$  is the  $\pi^0 pp$  vertex which is equal in Stapp formalism to (see Appendix A)

$$G_{(\pi^0 pp)} \sigma_b^p(p_p, p_b - p_p; p_b) = \frac{g_\pi}{\sqrt{2}} f(t) m (e - \tilde{V}_p V_b) \sigma_b^p, \quad (12)$$

where  $g_\pi$  is the  $\pi NN$  coupling constant, and  $f(t)$  is the pion form factor for which we take the monopole representation

$$f(t) = \frac{m_\pi^2 - \Lambda_\pi^2}{t - \Lambda_\pi^2}, \quad (13)$$

$\Lambda_\pi$  being the cut-off parameter. Defining the pion 'wave function' in the nucleon

$$\Phi_{(\pi^0 pp)} \sigma_b^p \equiv \frac{G_{(\pi^0 pp)} \sigma_b^p}{t - m_\pi^2} = \frac{m g_\pi}{\sqrt{2}} \left( \frac{1}{t - m_\pi^2} - \frac{1}{t - \Lambda_\pi^2} \right) (e - \tilde{V}_p V_b) \sigma_b^p, \quad (14)$$

and replacing the amplitude  $M_{(\pi^0 p \rightarrow K^+ \Lambda)}$  by the explored in the Rutherford Laboratory amplitude  $M_{(\pi^- p \rightarrow K^0 \Lambda)}$  [10], which are connected as follows

$$M_{(\pi^0 p \rightarrow K^+ \Lambda)} = M_{(\pi^- p \rightarrow K^0 \Lambda)} \sqrt{2} ,$$

we rewrite the eq.(11) as

$$\frac{i}{\sqrt{2}} M_{(\pi^- p \rightarrow K^0 \Lambda)} \sigma_t^{\Lambda} (p_{\Lambda}, p_K; p_t, p_b - p_p) \Phi_{(\pi^0 pp)} \sigma_b^p (p_p, p_b - p_p; p_b) . \quad (15)$$

The contribution of the graph  $b$  pictured in Fig. 2 is obtained from the expression (15) by the interchange of the beam and target quantities and we derive the final expression of the OPE contribution

$$M_{(OPE)} \sigma_b^{\Lambda} \sigma_t^p (p_p, p_{\Lambda}, p_K; p_b, p_t) = \frac{i}{\sqrt{2}} M_{(\pi^- p \rightarrow K^0 \Lambda)} \sigma_t^{\Lambda} (p_{\Lambda}, p_K; p_t, p_b - p_p) \Phi_{(\pi^0 pp)} \sigma_b^p (p_p, p_b - p_p; p_b) - (b \leftrightarrow t) , \quad (16)$$

where the relative minus sign is required by Pauli principle. In the Appendix A it is explained how the M-function expression (12) of the  $\pi^0 pp$  vertex is derived and how to obtain the M-function of the reaction  $\pi^- p \rightarrow K^0 \Lambda$  from the canonical flip and non-flip complex amplitudes  $G^s$  and  $H^s$ . We have taken into account only the S- and P-wave partial amplitudes in the partial wave development[11]

$$G^s = \frac{1}{q} \sum_{l=0}^{\infty} [(l+1)T_{l+} + lT_{l-}] P_l(x) ,$$

$$H^s = \frac{1}{q} \sum_{l=1}^{\infty} [T_{l+} - T_{l-}] P_l^1(x) , \quad (17)$$

where  $q = \sqrt{q_i q_f}$ ,  $q_{i,f}$  are the c.m. momenta in initial and final channels and  $x$  is the cosine of the c.m. scattering angle. Following the papers [10](Baker1978) we took

$$T_{0+}(s) = \frac{\Gamma \sqrt{xx'} m_p}{s - m_r^2 - im_r \Gamma} + \frac{2aq}{\sqrt{s}}$$

$$T_{1\pm}(s) = \frac{\Gamma \sqrt{xx'} e^{i\Phi} m_p}{s - m_r^2 - im_r \Gamma} ,$$

Table 2: Resonance parameters of the  $\pi^- p \rightarrow K^0 \Lambda$  amplitude

	$m_r$	$\Gamma_r$	$\sqrt{xx'}$	$\Phi$
$S_{11}$	1.68	0.09	-0.25	$0^0$
$P_{11}$	1.67	0.15	-0.115	$70^0$
$P_{13}$	1.75	0.40	-0.09	$20^0$

where

$$\Gamma = \Gamma_r \left( \frac{q}{q_r} \right)^{2l+1} \frac{2m_r}{\sqrt{s} + m_r} \frac{1 + (1.7q_r)^2}{1 + (1.7q)^2} \quad (18)$$

and the parameters are given in Tab. 2. Unfortunately the complex coefficient  $a$  describing the background is not presented by Rutherford Laboratory group, so we were to fit it to describe the differential cross sections at four c.m. energies 1.661, 1.683, 1.694 and 1.724 GeV given in [10](Baker1978).

The *virtuality of the initial*  $\pi^0$  is taken into account as follows. At first the amplitudes (17) are multiplied by the same form factor (13) as the  $\pi^0 pp$  vertex (12)

$$\begin{aligned} G^s &= \frac{f(t)}{\sqrt{q_i q_f}} \sum_{l=0}^{\infty} [(l+1)T_{l+} + lT_{l-}] P_l(x), \\ H^s &= \frac{f(t)}{\sqrt{q_i q_f}} \sum_{l=1}^{\infty} [T_{l+} - T_{l-}] P_l^1(x). \end{aligned} \quad (19)$$

In addition the c.m. momentum in initial channel  $\pi^0 p$  is calculated with the virtual mass of the pion  $t = (p_b - p_p)^2 < 0$ :

$$q_i = \frac{\sqrt{[(W_{K\Lambda} - m_p)^2 - t][(W_{K\Lambda} + m_p)^2 - t]}}{2W_{K\Lambda}}, \quad (20)$$

where  $W_{K\Lambda}$  is the invariant mass of the reaction.

## 2.2 FSI mechanism with the intermediate pion

The FSI graphs are shown in Figs. 1 *c, d*. Writing the contribution of, for example, the graph *c* in accordance with Feynman rules and putting the

proton 'spectator'  $p_s$  on the mass-shell we obtain <sup>2</sup>

$$\begin{aligned}
M_{FSI(\pi)c\sigma_t\sigma_b}^{\sigma_p\sigma_\Lambda} &= -i \int \frac{d\mathbf{p}_s}{(2\pi)^3 2E_s} \\
M_{(p_s\Lambda_v \rightarrow p\Lambda)\sigma_v}^{\sigma_\Lambda} \frac{1}{m_v^2 - m_\Lambda^2 + i\epsilon} M_{(\pi^0 p_t \rightarrow K^+\Lambda_v)\sigma_t}^{\sigma_v} \Phi_{(\pi^0 pp)\sigma_b}^{\sigma_s} &\approx \\
&\quad -i \frac{m_p}{W_{p\Lambda}} \int \frac{d\mathbf{p}_s}{(2\pi)^3 2E_s} \\
M_{(p_s\Lambda_v \rightarrow p\Lambda)\sigma_v}^{\sigma_\Lambda} \frac{1}{q_{cm}^2 - \xi^2 + i\epsilon} M_{(\pi^0 p_t \rightarrow K^+\Lambda_v)\sigma_t}^{\sigma_v} \Phi_{(\pi^0 pp)\sigma_b}^{\sigma_s}, &\quad (21)
\end{aligned}$$

where  $m_v$  is the mass of virtual  $\Lambda$  inside the triangle loop, the pion 'wave function' in the nucleon  $\Phi_{(\pi^0 pp)}$  is defined in eq. (14) and the non-relativistic approximation of the  $\Lambda$  propagator

$$m_v^2 - m_\Lambda^2 \approx \frac{W_{p\Lambda}}{m} (q_{cm}^2 - \xi^2)$$

is used. Here  $W_{p\Lambda} = \sqrt{s_{p\Lambda}}$ ,  $s_{p\Lambda} = p_{p\Lambda}^2$  and

$$\begin{aligned}
q_{cm} &= \frac{\sqrt{[(W_{p\Lambda} - m_p)^2 - m_\Lambda^2][(W_{p\Lambda} + m_p)^2 - m_\Lambda^2]}}{2W_{p\Lambda}}, \\
\xi &= \frac{\sqrt{[(W_{p\Lambda} - m_p)^2 - m_v^2][(W_{p\Lambda} + m_p)^2 - m_v^2]}}{2W_{p\Lambda}}
\end{aligned} \quad (22)$$

are the c.m. momenta of  $\Lambda$  after (on-shell) and before (off-shell) the scattering.

Simplifications are necessary in order to calculate the integral (21) since it requires a knowledge of the off-shell  $\pi^0 p \rightarrow K^+ \Lambda$  and  $p\Lambda$  amplitudes. In this we have followed the paper [12] with some modification described in [13]. Namely, these amplitudes are taken out of the integral sign at some momentum  $p_s^0$  placed on the singular surface of the integral corresponding to the mass-shell of the virtual  $\Lambda$ .

When a separable potentials for  $p\Lambda$  scattering are assumed for each partial-wave state the relation

$$M_{p\Lambda}^{off} = f(m_v^2) M_{p\Lambda}^{on} \quad (23)$$

---

<sup>2</sup>As it was explained above, the same index  $\sigma_v$ , spin projection of the virtual  $\Lambda$ , at the up and down positions stands for a summation over this index.

	Set A-1	Set A-2	Set A-3	Set B-1	Set B-2
$^1S_0$	0.209	0.256	0.239	0.257	0.258
$^3S_1$	0.217	0.246	0.252	0.247	0.243

Table 3: Parameter  $\beta(\text{GeV}/c)$  of separable  $p\Lambda$  potential by Y.Takahashi et al.

is strictly valid. The usual form of the form factor  $f$  is

$$f(m_v^2) = \frac{q_{c.m.}^2 + \beta^2}{\xi^2 + \beta^2}, \quad (24)$$

where  $\beta$  is the cut-off parameter. Near threshold two S-waves,  $^1S_0$  and  $^3S_1$ , give the major contribution. In the paper[14] different sets of separable  $p\Lambda$  potential were found with good fits to the cross-section. They are presented in Tab. 3. Following this table we neglected the difference between the spin singlet and spin triplet S-wave parameters and took the form factor (24) for the whole low-energy amplitude with  $\beta$  varying in the region  $0.1 \leq \beta \leq 0.3$  GeV/c. Taking into account that

$$\frac{f(m_v^2)}{q_{cm}^2 - \xi^2 + i\epsilon} = \left[ -\frac{1}{\xi^2 - q_{cm}^2 - i\epsilon} + \frac{1}{\xi^2 + \beta^2} \right]$$

the eq. (21) can be rewritten as

$$M_{FSI(\pi)c\sigma_t\sigma_b}^{\sigma_p\sigma_\Lambda} \approx -i \frac{m_p}{W_{p\Lambda}} \int \frac{d\mathbf{p}_s}{(2\pi)^3 2E_s}$$

$$M_{(p_s\Lambda_v \rightarrow p\Lambda)\sigma_v}^{\sigma_\Lambda} M_{(\pi^0 p_t \rightarrow K^+\Lambda_v)\sigma_t}^{\sigma_v} \Phi_{(\pi^0 pp)\sigma_b}^{\sigma_s} \left[ -\frac{1}{\xi^2 - q_{cm}^2 - i\epsilon} + \frac{1}{\xi^2 + \beta^2} \right]. \quad (25)$$

We took the half-off-shell  $\pi^0 p \rightarrow K^+ \Lambda$  and on-shell part of  $p\Lambda$  amplitudes (23) out of the integral sign at specially chosen momenta. Following the argumentation of [13] the best choice for the graph  $c$  is the maximal momentum of the on-shell loop proton  $p_s$ , which is directed along  $\mathbf{p}_\Lambda$  and is equal to

$$\mathbf{p}_{p(+)} = \mathbf{p}_{p\Lambda} \left( \frac{E_p^{cm}}{W_{p\Lambda}} + \frac{E_{p\Lambda}}{W_{p\Lambda}} \frac{q^{cm}}{p_{p\Lambda}} \right).$$

In this case  $\Lambda$  is on-shell too and has correspondingly the minimal momentum  $p_{\Lambda(-)}$

$$\mathbf{p}_{\Lambda(-)} = \mathbf{p}_{p\Lambda} \left( \frac{E_\Lambda^{cm}}{W_{p\Lambda}} - \frac{E_{p\Lambda}}{W_{p\Lambda}} \frac{q^{cm}}{p_{p\Lambda}} \right).$$

Here  $E_p^{cm}$  and  $E_\Lambda^{cm}$  are c.m. energies of the proton and  $\Lambda$  respectively. Under these assumptions we can rewrite eq.(25) as follows

$$\begin{aligned}
& M_{FSI(\pi)c\sigma_b\sigma_t}^{\sigma_\Lambda\sigma_p}(p_p, p_\Lambda, p_k; p_b, p_t) = \\
& -iM_{(p\Lambda)\sigma_s\sigma_v}^{\sigma_p\sigma_\Lambda}(p_p, p_\Lambda; p_{p(+)}, p_{\Lambda(-)})(e - \tilde{V}_{p(+)}V_b)_{\sigma_b}^{\sigma_s} \\
& M_{(\pi^0 p \rightarrow K^+\Lambda)\sigma_t}^{\sigma_v}(p_K, p_{\Lambda(-)}; p_b - p_{p(+)}, p_t) \cdot F(s_{p\Lambda}, t), \tag{26}
\end{aligned}$$

where  $t = (p_t - p_K)^2$  and

$$\begin{aligned}
F(s_{p\Lambda}, t) \equiv \frac{g_\pi m^2}{W_{p\Lambda}\sqrt{2}} \int \frac{d\mathbf{p}_s}{(2\pi)^3 2E_s} \left[ \frac{1}{(p_b - p_s)^2 - m_\pi^2} - \frac{1}{(p_b - p_s)^2 - \Lambda_\pi^2} \right] \\
\left[ -\frac{1}{\xi^2 - q_{cm}^2 - i\epsilon} + \frac{1}{\xi^2 + \beta^2} \right]. \tag{27}
\end{aligned}$$

In Appendix B the details of the calculation of the integral (27) are given. The result is

$$\begin{aligned}
F(s_{p\Lambda}, t) \approx \frac{g_\pi m}{32\pi W_{p\Lambda} q_b \sqrt{2}} \sum_j C_j \\
\left[ -i \ln \frac{\xi_{j+}^2 + \alpha_j^2}{\xi_{j-}^2 + \alpha_j^2} - 2 \arctan \frac{\xi_{j+}}{\alpha_j} - 2 \arctan \frac{\xi_{j-}}{\alpha_j} + 4 \arctan \frac{\xi_{j+} + \xi_{j-}}{2(\beta + \alpha_j)} \right], \tag{28}
\end{aligned}$$

where  $q_b$  is the c.m. momentum of the system  $p_b + (p_t - p_K)$  equal to

$$q_b = \frac{\sqrt{[(W_{p\Lambda} + m)^2 - t][(W_{p\Lambda} - m)^2 - t]}}{2W_{p\Lambda}}, \quad t = (p_t - p_K)^2 \tag{29}$$

and

$$\begin{aligned}
\alpha_1 = E_b \sqrt{1 - \left(1 - \frac{m_\pi^2}{2m^2}\right)^2}, \quad \alpha_2 = E_b \sqrt{1 - \left(1 - \frac{\Lambda_\pi^2}{2m^2}\right)^2}, \\
\xi_{1\pm} = q_b \left(1 - \frac{m_\pi^2}{2m^2}\right) \pm q_{c.m.}, \quad \xi_{2\pm} = q_b \left(1 - \frac{\Lambda_\pi^2}{2m^2}\right) \pm q_{c.m.}, \tag{30}
\end{aligned}$$

$$C_1 = 1, \quad C_2 = -1. \tag{31}$$

The contribution of the second FSI graph with virtual pion (Fig. 1 *d*) is derived by the interchange  $b \leftrightarrow t$ :

$$\begin{aligned}
& M_{FSI(\pi)d\sigma_b\sigma_t}^{\sigma_\Lambda\sigma_p}(p_p, p_\Lambda, p_k; p_b, p_t) = \\
& -iM_{(p\Lambda)\sigma_s\sigma_v}^{\sigma_p\sigma_\Lambda}(p_p, p_\Lambda; p_{p(-)}, p_{\Lambda(+)})(e - \tilde{V}_{p(-)}V_t)_{\sigma_b}^{\sigma_s} \\
& M_{(\pi^0 p \rightarrow K^+\Lambda)\sigma_t}^{\sigma_v}(p_K, p_{\Lambda(+)}; p_t - p_{p(-)}, p_b) \cdot F(s_{p\Lambda}, t), \tag{32}
\end{aligned}$$

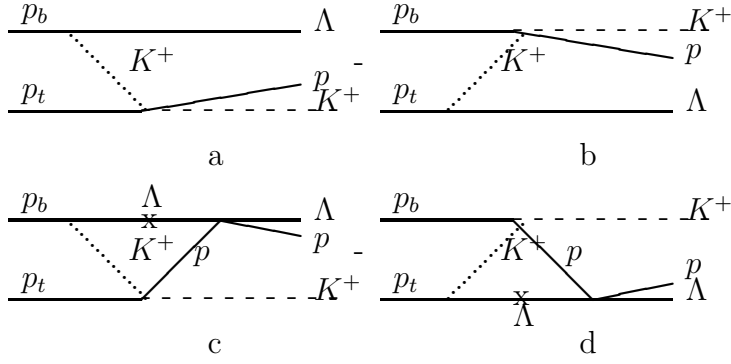


Figure 2: OKE (a,b) and FSI diagrams (c,d)

where  $t = (p_K - p_b)^2$ , and

$$\mathbf{p}_{p(-)} = \mathbf{p}_{p\Lambda} \left( \frac{E_p^{cm}}{W_{p\Lambda}} - \frac{E_{p\Lambda}}{W_{p\Lambda}} \frac{q^{cm}}{p_{p\Lambda}} \right), \quad \mathbf{p}_{\Lambda(+)} = \mathbf{p}_{p\Lambda} \left( \frac{E_\Lambda^{cm}}{W_{p\Lambda}} - \frac{E_{p\Lambda}}{W_{p\Lambda}} \frac{q^{cm}}{p_{p\Lambda}} \right). \quad (33)$$

### 3 Kaon exchange mechanisms

#### 3.1 One Kaon Exchange amplitude

The OKE graphs are shown in Figures 2a,b. The final expression of the OKE contribution is similar to eq.(16)

$$M_{(OKE)_{\sigma_b \sigma_t}^{\sigma_\Lambda \sigma_p}}(p_p, p_\Lambda, p_K; p_b, p_t) = iM_{(K+p)_{\sigma_t}^{\sigma_p}}(p_p, p_K; p_t, p_b - p_\Lambda) \Phi_{(K+p\Lambda)_{\sigma_b}^{\sigma_\Lambda}}(p_\Lambda, p_b - p_\Lambda; p_b) - (b \leftrightarrow t). \quad (34)$$

The kaon 'wave function' in the  $K^+ p \Lambda$  vertex is equal to

$$\Phi_{(K+p\Lambda)_{\sigma_b}^{\sigma_\Lambda}} = g_K \sqrt{m m_\Lambda} \left( \frac{1}{t - m_K^2} - \frac{1}{t - \Lambda_K^2} \right) (e - \tilde{V}_\Lambda V_b)_{\sigma_b}^{\sigma_\Lambda}, \quad (35)$$

where  $t = (p_\Lambda - p_b)^2$ ,  $g_K$  is the  $K^+ p \Lambda$  coupling constant [15] and  $\Lambda_K$  is the cut-off parameter in the monopole form factor (see eq. (13) for virtual pion of virtual  $K$ ).

The  $M_{(K+p)}$  is the half-off-shell  $K^+ p \rightarrow K^+ p$  amplitude, the M-function of which is derived from the canonical amplitude in the same way as  $M_{(\pi^- p \rightarrow K^0 \Lambda)}$  (see the previous section and Appendix A). In order to calculate the canonical flip and non-flip amplitudes we have utilized the isotriplet partial-wave amplitudes below 1.5 GeV/c obtained in the phase shift analysis by Martin [16].

### 3.2 FSI with intermediate kaon

For the graph in Fig. 2 *c* we have

$$M_{FSI(K)c_{\sigma_b \sigma_t}^{\sigma_\Lambda \sigma_p}}(p_p, p_\Lambda, p_k; p_b, p_t) = -iM_{(p\Lambda)_{\sigma_v \sigma_s}^{\sigma_p \sigma_\Lambda}}(p_p, p_\Lambda; p_{p(-)}, p_{\Lambda(+)})(e - \tilde{V}_{\Lambda(+)} V_b)_{\sigma_b}^{\sigma_s} M_{(K+p)_{\sigma_t}^{\sigma_v}}(p_K, p_{p(-)}; p_b - p_{\Lambda(+)}, p_t) \cdot F_K(s_{p\Lambda}, t), \quad (36)$$

where  $t = (p_K - p_t)^2$  and

$$F(s_{p\Lambda}, t) = \frac{g_K m_\Lambda \sqrt{m m_\Lambda}}{W_{p\Lambda}} \int \frac{d\mathbf{p}_s}{(2\pi)^3 2E_s} \left[ \frac{1}{(p_b - p_s)^2 - m_K^2} - \frac{1}{(p_b - p_s)^2 - \Lambda_K^2} \right] \left[ -\frac{1}{\xi^2 - q_{cm}^2 - i\epsilon} + \frac{1}{\xi^2 + \beta^2} \right], \quad (37)$$

where now the integration is performed over the 3-momentum  $\mathbf{p}_s$  of the on-shell  $\Lambda$  in the triangle loop. Manipulations similar to those described in Appendix B for the pion case result in

$$F_K(s_{p\Lambda}, t) \approx \frac{g_K}{32\pi q} \sqrt{\frac{m_\Lambda^3}{m^3}} \sum_j C_j \left[ -i \ln \frac{\xi_{j+}^2 + \alpha_j^2}{\xi_{j-}^2 + \alpha_j^2} - 2 \arctan \frac{\xi_{j+}}{\alpha_j} - 2 \arctan \frac{\xi_{j-}}{\alpha_j} + 4 \arctan \frac{\xi_{j+} + \xi_{j-}}{2(\beta + \alpha_j)} \right], \quad (38)$$

where

$$\alpha_1 = E_b \sqrt{1 - \frac{(m^2 + m_\Lambda^2 - m_K^2)^2}{4m^2 m_\Lambda^2}}, \quad \alpha_2 = E_b \sqrt{1 - \frac{(m^2 + m_\Lambda^2 - \Lambda_K^2)^2}{4m^2 m_\Lambda^2}},$$

$$\xi_{1\pm} = q_b \frac{m^2 + m_\Lambda^2 - m_K^2}{2mm_\Lambda} \pm q_{c.m.}, \quad \xi_{2\pm} = q_b \frac{m^2 + m_\Lambda^2 - \Lambda_K^2}{2mm_\Lambda} \pm q_{c.m.}, \quad (39)$$

$$C_1 = 1, \quad C_2 = -1, \quad (40)$$

and  $q = \frac{W_{p\Lambda}}{m} q_b$ . The contribution of the second FSI graph with virtual kaon (Fig. 2 *d*) is derived by the interchange  $b \leftrightarrow t$ .

## 4 Results and discussion

Let us start with the total cross sections for OKE+FSI mechanism. Free parameters in this case are  $g_K$  -  $K^+p\Lambda$  coupling constant,  $\Lambda_K$  - the cut-off parameter in the monopole form factor of virtual  $K$  and  $\beta$  - the cut-off parameter in the form factor in half-off shell  $p\Lambda$  interaction. The cut-off parameter  $\Lambda_K = 0.9$  had been chosen and with  $g_K = -4.17\sqrt{4\pi} = -14.78$  GeV, the value recommended in the paper [15], it appeared that the experimental data presented in Tab. 1 are fairly well described by only OKE mechanism. Still to find place for the FSI contributions, from the one hand the coupling constant  $g_K$  had been minimally decreased to the value  $g_K = -11.8$  in order to

stay in agreement with SU(3) predictions for the kaon-hyperon-nucleon coupling constants (see [15]), and from the other hand the FSI contributions had been minimized by choosing rather small value of the half-off shell  $p\Lambda$  cut-off parameter:  $\beta = 0.1$ . The resulting total cross sections versus the excess energy  $Q = W - m_p - m_\Lambda - m_K$  are shown as double logarithmic plot in Fig. 3. It is seen that OKE+FSI(K) model alone with the plausible parameters

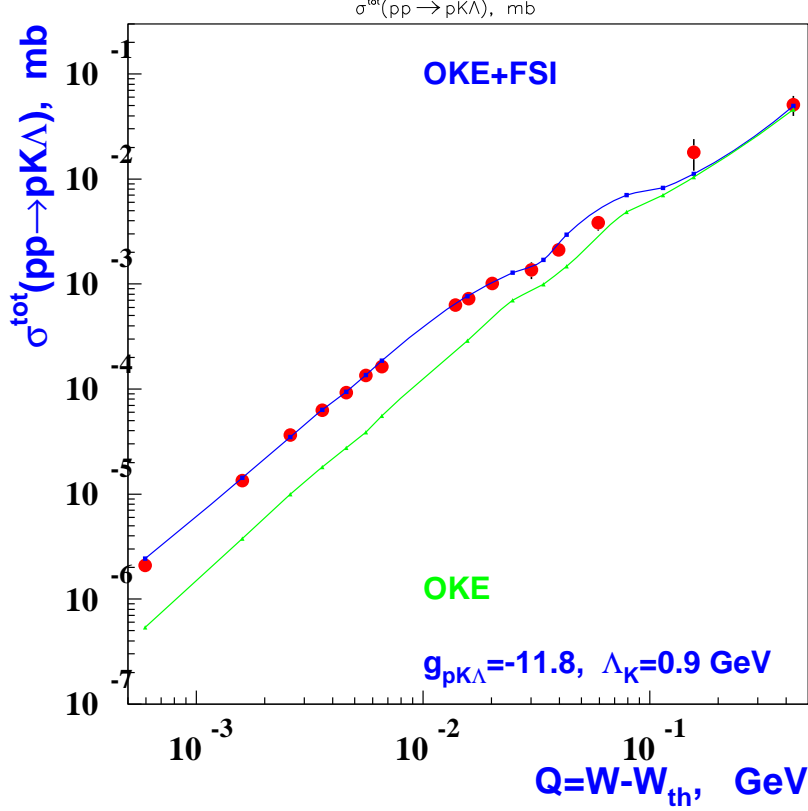


Figure 3: Red circles are the experimental total  $pp \rightarrow p\Lambda K^+$  cross sections versus the excess energy  $Q = W - W_{th}$ . Green curve presents the calculations in the frame of OKE model. Blue curve - the calculations in the frame of OKE+FSI model.

describes very well the experimental data, which is already a hint in favor

of kaon mechanism dominance in  $pp \rightarrow p\Lambda K^+$  reaction. The  $Q$  behavior of the difference between pure OKE and OKE+FSI(K) curves demonstrates, that near the threshold FSI contribution is compatible with the OKE one, whereas at higher  $Q$  the OKE becomes the dominating mechanism.

Though the kaon mechanism seems to be enough we should find place for the OPE+FSI( $\pi$ ) graphs. Free parameters in this case are  $g_\pi$  - the  $\pi NN$  coupling constant and  $\Lambda_\pi$  - the cut-off parameter in the monopole form factor (13) of virtual  $\pi$ . The cut-off parameter in the form factor in half-off shell  $p\Lambda$  interaction  $\beta = 0.1$  was fixed by OKE+FSI(K) fit. The well established value  $g_\pi \simeq 13.5$  ( $g_\pi^2/4\pi = 14.5$ ) had been fixed. Then it appeared that using the common accepted  $\Lambda_\pi \approx 1$  GeV results in high OPE contribution near the threshold which would be impossible to compensate by other mechanisms. We have decreased the cut-off parameter  $\Lambda_\pi$  to the value  $\Lambda_\pi = 0.515$  GeV. The resulting plots are shown in Fig. 4. It is seen that only for  $Q < 1.7$  MeV the contribution of OPE+FSI( $\pi$ ) graphs exceeds experimental data and there is no possibility to decrease this contribution. For higher  $Q$  the OPE+FSI( $\pi$ ) contribution to the experimental data is negligible.

The applying the full model, including the both kaon and pion mechanisms, with the parameters fixed above had shown that in case of "constructive" interference

$$M = M_{OPE} + M_{OKE} + M_{FSI(\pi)} + M_{FSI(K)}$$

the model total cross sections exceed the measured ones, the difference being especially large near the threshold. In contrast, the choice of destructive interference

$$M = -M_{OPE} + M_{OKE} - M_{FSI(\pi)} + M_{FSI(K)}$$

results in fairly well description of the data, which is demonstrated in Fig. 5. This our observation confirms the conclusion of the Juelich group [7] that the experimental data require a destructive interference between  $\pi^0$  and  $K$  exchange contributions.

In conclusion we can confirm the main features of the  $pp \rightarrow p\Lambda K^+$  scattering at low and intermediate energies observed in the previous studies [4, 7, 8]: the kaon mechanism dominance at intermediate energies, the compatibility of all mechanisms near the threshold and the destructive interference between kaon and pion amplitudes. The model presented in this work describes sufficiently well the measured total cross sections  $pp \rightarrow p\Lambda K^+$  in the wide interval

of the excess energy  $Q = W - m - m_\Lambda - m_K$ :  $0.68 \leq Q \leq 430$  MeV. Our further plans are to apply this model for the description for the analysis of the proton and kaon spectra in  $pp \rightarrow p\Lambda K$  reaction at COSY energies [9] and to make predictions for the polarization observables at these energies.

## Acknowledgement

The author thanks V.Koptev for the fruitful discussions and cooperation during performing of this work.

## A M-functions

When calculating a coherent sums of various mechanisms one needs in principle to transform the matrices of corresponding amplitudes from center of mass frames to the common laboratory frame. These transformations depend on the spin basis chosen for the one-fermion states. Usually the canonical or helicity basis are used which are transformed with unitary two by two matrices depending on a fermion momentum. They are so called Wigner rotations. The covariant basis [17]transforming independently of the particle momentum by the unimodular two by two matrices is free from this deficiency. Amplitudes in the covariant basis are usually referred to as the M-functions of Stapp. The covariant formalism of the M-functions developed by Stapp [17] is based on the matrices  $\sigma^\mu = (1, \vec{\sigma})$  and  $\tilde{\sigma}^\mu = (1, -\vec{\sigma})$ , where  $\vec{\sigma}$  are the standard Pauli matrices. With each momentum  $P^\mu$  of the reaction two by two matrices  $\tilde{P} \equiv P^\mu \tilde{\sigma}_\mu$  and  $P \equiv P^\mu \sigma_\mu$  are associated. The products  $\tilde{P}_i P_j$  of these matrices are the elements from which the M-functions are built. The matrices  $\tilde{V}_i$  and  $V_i$  associated with the four-velocity of the i-th particle, serve as the metric tensors of the particle when performing the contraction over this index (traces, successive processes).

Let us explain the M-function expression (12) of the  $\pi^0 pp$  vertex and how to obtain the M-function of the reaction  $\pi^- p \rightarrow K^0 \Lambda$  from the canonical amplitude. As to the  $\pi^0 pp$  vertex it is nothing but the usual expression  $g\bar{u}_f \gamma_5 u_i$  with the exception that the modified Dirac bispinors are used. In the Weyl representation they are equal to

$$u^\alpha_b = \sqrt{m} \begin{pmatrix} e_b^a \\ V_{\bar{a}b} \end{pmatrix}, \quad \bar{u}_\alpha^b = \sqrt{m} \begin{pmatrix} e_a^b & V^{b\bar{a}} \end{pmatrix}. \quad (41)$$

In the Weyl representation the  $\gamma_5$ - matrix looks like

$$\gamma_5 = \begin{pmatrix} e & 0 \\ 0 & -e \end{pmatrix}$$

and the amplitude of transition between real states with the production of the pseudoscalar is equal to

$$M_b^a(p_f, q; p_i) = g \bar{u}_\alpha^a \gamma_5^\alpha u_b^\beta = g \sqrt{m_f m_i} (e_b^a - V_f^{a\bar{c}} V_{i\bar{c}b}) ,$$

or in indexless form

$$M(p_f, q; p_i) = g \bar{u}_f \gamma_5 u_i = g \sqrt{m_f m_i} (e - \tilde{V}_f V_i) , \quad (42)$$

which explains the eq.(12).

As to the M-function of the  $0\frac{1}{2} \rightarrow 0\frac{1}{2}$  reaction it is possible to represent as

$$M = G^m b_1 + H^m b_2 , \quad (43)$$

where  $G^m$  and  $H^m$  are the complex functions and  $b_{1,2}$  are the basis M-functions equal to

$$b_1 \equiv \frac{e + \tilde{V}_f V_i}{\sqrt{(M_1, M_1)}} , \quad b_2 \equiv \frac{\alpha(e + \tilde{V}_f V_i) + (\tilde{V}_f V + \tilde{V} V_i)}{\sqrt{(M_2, M_2)}} . \quad (44)$$

Here  $V, V_i$  and  $V_f$  are the four-velocities of the c.m., of initial and of final spinor particle. The coefficient  $\alpha$  and the normalization coefficients  $\sqrt{(M_i, M_i)}$  are equal to

$$\begin{aligned} \alpha &= -2 \frac{(V, V_i + V_f)}{(V_i + V_f)^2} , \\ (M_1, M_1) &= 2 [1 + (V_f, V_i)] , \\ (M_2, M_2) &= 2 \frac{[1 - (V, V_f)^2][1 - (V, V_i)^2] - [(V_f, V_i) - (V, V_f)(V, V_i)]^2}{1 + (V_f, V_i)} . \end{aligned}$$

In this case the corresponding cross section is equal to  $|G^m|^2 + |H^m|^2$ . Thus there is the unitary connection between  $G^m, H^m$  and the canonical flip and non-flip c.m.  $S$ -matrix amplitudes

$$S = G^s + i H^s \hat{n} , \quad \hat{n} \equiv n^k e_k , \quad \vec{n} = \frac{\vec{k}_i \times \vec{k}_f}{|\vec{k}_i \times \vec{k}_f|} ,$$

where  $\vec{k}_{i,f}$  are initial and final c.m. momenta [11]. It is

$$\begin{aligned} G^m &= \cos \frac{\varphi}{2} G^s - \sin \frac{\varphi}{2} H^s, \\ H^m &= \sin \frac{\varphi}{2} G^s + \cos \frac{\varphi}{2} H^s, \end{aligned}$$

where the angle  $\varphi$  is determined by

$$e^{i\frac{\varphi}{2}} = \sqrt{\frac{\omega_0 - \omega}{\omega_0 - \omega^{-1}}}, \quad \omega_0 \equiv \sqrt{\frac{(V, V_f) + 1}{(V, V_f) - 1} \frac{(V, V_i) + 1}{(V, V_i) - 1}}, \quad \omega \equiv e^{i\theta}. \quad (45)$$

The  $\theta$  is the c.m. scattering angle.

## B Calculation of the transitive form factor F

Let us chose the  $p\Lambda$  c.m. system. Then

$$\begin{aligned} p_b &= (E_b, \mathbf{q}_b), \quad \mathbf{p}_s = \xi, \quad (p_b - p_s)^2 = 2m^2 - 2E_b E_\xi + 2q_b \xi x, \\ E_b &= \frac{s_{p\Lambda} + m^2 - t}{2W_{p\Lambda}}, \quad q_b = \frac{\sqrt{[(W_{p\Lambda} + m)^2 - t][(W_{p\Lambda} - m)^2 - t]}}{2W_{p\Lambda}}. \end{aligned}$$

Choosing z-axis along  $\mathbf{q}_b$ , taking into account  $d\xi = d\phi dx \xi^2 d\xi$  and integrating with respect to azimuthal angle and  $x$  we derive

$$\begin{aligned} F(s_{p\Lambda}, t) &= \frac{g_\pi}{\sqrt{216}\pi^2 q} \int_0^\infty \xi d\xi \left[ -\frac{1}{\xi^2 - q_{cm}^2 - i\epsilon} + \frac{1}{\xi^2 + \beta^2} \right] \cdot \\ &\left[ \ln \frac{2E_b E_\xi - 2q_b \xi - 2m^2 + m_\pi^2}{2E_b E_\xi + 2q_b \xi - 2m^2 + m_\pi^2} - \ln \frac{2E_b E_\xi - 2q_b \xi - 2m^2 + \Lambda_\pi^2}{2E_b E_\xi + 2q_b \xi - 2m^2 + \Lambda_\pi^2} \right], \quad (46) \end{aligned}$$

where  $q = \frac{W_{p\Lambda}}{m} q_b$ . This integral can be computed if we replace the arguments of the logarithms by the parabola with the roots coinciding with the roots of these arguments. They are complex and equal to

$$\begin{aligned} \xi(m_\pi)_\pm &= q_b \left(1 - \frac{m_\pi^2}{2m^2}\right) \pm iE_b \sqrt{1 - \left(1 - \frac{m_\pi^2}{2m^2}\right)^2}, \\ \xi(\Lambda_\pi)_\pm &= q_b \left(1 - \frac{\Lambda_\pi^2}{2m^2}\right) \pm iE_b \sqrt{1 - \left(1 - \frac{\Lambda_\pi^2}{2m^2}\right)^2} \end{aligned} \quad (47)$$

and we have to calculate

$$F(s_{p\Lambda}, t) = \frac{g_\pi}{64\pi^2 q \sqrt{2}} \int_{-\infty}^{\infty} d\xi \left[ -\frac{1}{\xi - q_{cm} - i\epsilon} - \frac{1}{\xi + q_{cm} + i\epsilon} + \frac{1}{\xi + i\beta} + \frac{1}{\xi - i\beta} \right] \cdot \left[ \ln \frac{\xi - \xi(m_\pi)_+}{\xi + \xi(m_\pi)_-} + \ln \frac{\xi - \xi(m_\pi)_-}{\xi + \xi(m_\pi)_+} - \ln \frac{\xi - \xi(\Lambda_\pi)_+}{\xi + \xi(\Lambda_\pi)_-} - \ln \frac{\xi - \xi(\Lambda_\pi)_-}{\xi + \xi(\Lambda_\pi)_+} \right]. \quad (48)$$

Here arguments of the each logarithms has singularities only in the lower or upper half-plane. The first and the third logarithms are free from singularities in lower half-plane and closing the contour for them in lower half-plane we meet the poles at  $-q_{cm} - i\epsilon$  and  $-i\beta$ . In contrast the second and fourth logarithms pick up in upper half-plane the poles at  $q_{cm} + i\epsilon$  and  $i\beta$ . This yields

$$F(s_{p\Lambda}, t) = \frac{g_\pi}{\sqrt{2}16\pi q} i \left( -\ln \frac{-q_{cm} - i\epsilon - \xi(m_\pi)_+}{-q_{cm} - i\epsilon + \xi(m_\pi)_-} + \ln \frac{-q_{cm} - i\epsilon - \xi(\Lambda_\pi)_+}{-q_{cm} - i\epsilon + \xi(\Lambda_\pi)_-} + \ln \frac{-i\beta - \xi(m_\pi)_+}{-i\beta + \xi(m_\pi)_-} - \ln \frac{-i\beta - \xi(\Lambda_\pi)_+}{-i\beta + \xi(\Lambda_\pi)_-} \right) = \frac{g_\pi}{16\pi q} i \left( -\ln \frac{-iq_{cm} - i\xi(m_\pi)_+}{-iq_{cm} + i\xi(m_\pi)_-} + \ln \frac{-iq_{cm} - i\xi(\Lambda_\pi)_+}{-iq_{cm} + i\xi(\Lambda_\pi)_-} + \ln \frac{\beta - i\xi(m_\pi)_+}{\beta + i\xi(m_\pi)_-} - \ln \frac{\beta - i\xi(\Lambda_\pi)_+}{\beta + i\xi(\Lambda_\pi)_-} \right). \quad (49)$$

Defining

$$\alpha_1 = E_b \sqrt{1 - \left(1 - \frac{m_\pi^2}{2m^2}\right)^2}, \quad \alpha_2 = E_b \sqrt{1 - \left(1 - \frac{\Lambda_\pi^2}{2m^2}\right)^2},$$

$$\xi_{1\pm} = q_b \left(1 - \frac{m_\pi^2}{2m^2}\right) \pm q_{c.m.}, \quad \xi_{2\pm} = q_b \left(1 - \frac{\Lambda_\pi^2}{2m^2}\right) \pm q_{c.m.}, \quad (50)$$

$$C_1 = 1, \quad C_2 = -1, \quad (51)$$

we can write the final expression in the form similar to that of Laget

$$F(s_{p\Lambda}, t) = \frac{g_\pi}{32\pi q \sqrt{2}} \sum_j C_j \left[ -i \ln \frac{\xi_{j+}^2 + \alpha_j^2}{\xi_{j-}^2 + \alpha_j^2} - 2 \arctan \frac{\xi_{j+}}{\alpha_j} - 2 \arctan \frac{\xi_{j-}}{\alpha_j} + 4 \arctan \frac{\xi_{j+} + \xi_{j-}}{2(\beta + \alpha_j)} \right]. \quad (52)$$

## References

- [1] J.T.Balewski et al., Total Cross Section of the Reaction  $pp \rightarrow pK^+\Lambda$  Close to Threshold *Phys.Lett.* **B420**(1998)211.
- [2] S. Sewerin et al., Comparison of  $\Lambda$  and  $\Sigma^0$  Production near Threshold in Proton-Proton Collision. *Phys.Rev. Lett.* **83**(1999)682.
- [3] P.Kowina et al., Energy dependence of the  $\Lambda/\Sigma^0$  production cross-section ratio in p-p interactions. *Eur.Phys.J.* **A22**(2004)293.
- [4] J.M.Laget, Strangeness production in nucleon-nucleon collisions. *Phys.Lett.* **B259**(1991)23.
- [5] J.M.Laget, Strangeness production by electromagnetic and hadronic probes. *Nucl.Phys.* **A691**(2001)11.
- [6] A. Baldini, V.Flamino, W.G.Moorhead and D.R.O.Morrison, Total Cross Section of the Reaction  $pp \rightarrow pK^+\Lambda$  at  $T_p = 2.02$  and  $T_p = 2.85$  GeV. Landolt-Boernstein, *New Series* **12**(1998).
- [7] A.M.Gasparian, J.Heidenbauer, C.Hanhart, L.Kondratyuk and J.Speth, Near threshold  $\Lambda$  and  $\Sigma$  production in  $pp$  collisions. *nucl-th/000608*, 2000.
- [8] A.Sibirtsev, J.Heidenbauer, H.-W.Hammer and S.Krewald, Resonances and final state interactions in the reaction  $pp \rightarrow pK^+\Lambda$ . *nucl-th/0512058*,2005
- [9] V.Koptev and Yu.Valdau, private communications.
- [10] R.D.Baker et al., *Nucl. Phys.* **B126**(1977)365, *Nucl. Phys.* **B141**(1978)29, *Nucl. Phys.* **B222**(1983)389. D.H.Saxon et al., *Nucl. Phys.* **B162**(1980)522.
- [11] G.Hohler et al., Handbook of Pion-Nucleon Scattering **12-1**(1979)1
- [12] J.M.Laget, *Nucl. Phys.* **A296**(1978)389.
- [13] O.Grebenyuk, Preprint PNPI **2648** (2005) 47 p., *nucl-th/0511081*(2005)
- [14] Y.Takahashi et al., *Nucl. Phys.* **A336**(1980)347.

- [15] R.A.Adelseck and B.Saghai, Kaon photoproduction: Data consistency, coupling constants and polarization observables. *Phys.Rev.* **C42** (1990) 108.
- [16] B.R.Martin, Kaon-nucleon partial-wave amplitudes below 1.5 Gev/c for  $I = 0$  and 1. *Nucl. Phys.* **B94**(1975)413.
- [17] Henry P.Stapp, *Phys.Rev.* **D27** (1983) 2445.

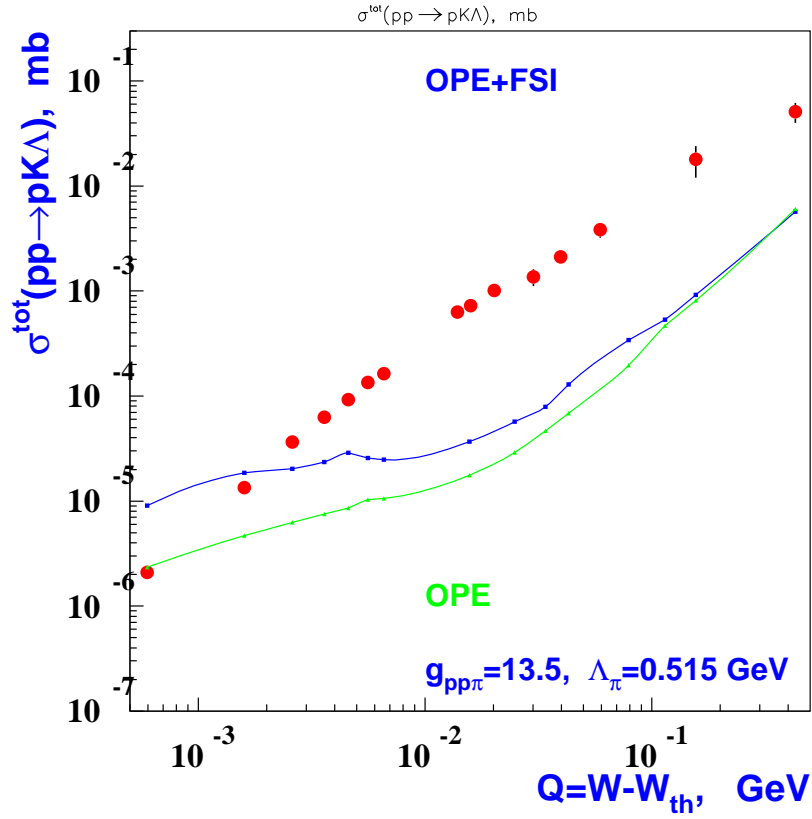


Figure 4: Red circles are the experimental total  $pp \rightarrow p\Lambda K^+$  cross sections versus the excess energy  $Q = W - W_{th}$ . Green curve presents the calculations in the frame of OPE model. Blue curve - the calculations in the frame of OPE+FSI( $\pi$ ) model.

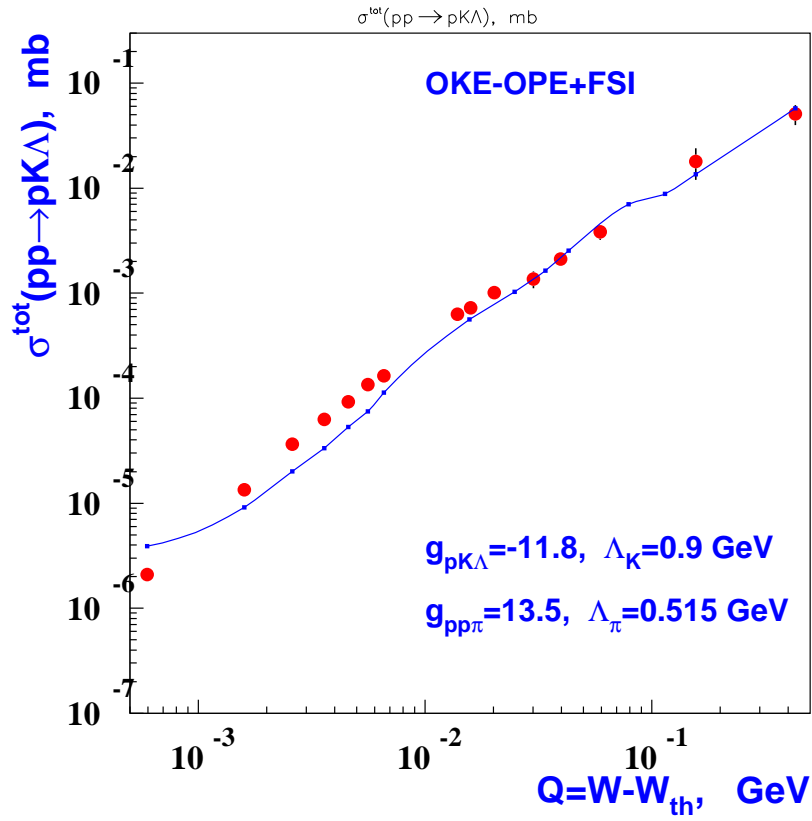


Figure 5: Red circles are the experimental total  $pp \rightarrow p\Lambda K^+$  cross sections versus the excess energy  $Q = W - W_{th}$ . Blue curve - the calculations in the frame of full OKE-OPE model (destructive interference)